ISBN: 978-3-95450-262-2 ISSN: 2673-5350 doi: 10.18429/JACoW-IBIC2025-MOBI01

TRANSVERSE MOMENTUM MEASURING SYSTEMS: THE CRYOGENIC MOMENTATRON AND TESS

G. Adhikari*, T. Vecchione, Stanford Linear Accelerator Center, USA
I-J Shan, W. A. Schroeder, University of Chicago, Illinois, USA
L. B. Jones†, H. M. Churn, UKRI, STFC Daresbury Laboratory, UK

Abstract

Photocathode performance optimization is crucial to the operation of X-ray Free Electron Laser (FEL) facilities such as LCLS-II and the future UK XFEL as the initial photoelectron phase-space distribution directly impacts x-ray generation efficiency in the undulator. Key photocathode parameters such as transverse emittance and quantum efficiency are routinely measured to monitor and improve performance, but other metrics are influenced by the photocathode material such as operating temperature, vacuum and RF environmental conditions and the characteristics of laser illumination (e.g., wavelength, and pulse energy, duration, and repetition rate). To better understand these factors, SLAC has developed a laboratory-based Cryogenic Momentatron system to measure the emission properties of photocathodes at temperatures between 30 K and 300 K using 200 – 800 nm wavelength-tunable light. The system's design and initial commissioning performance have been validated through simulations and error analysis, confirming its reliability for photocathode characterization. We present measurements taken at SLAC, along with complementary data for Cs_2Te obtained using the TESS system at Daresbury Laboratory - a similar photocathode characterization tool. These results provide valuable insights into photoemission physics that may be leveraged to optimize photocathode performance and thus that of X-ray FELs.

ENERGY / MOMENTUM MEASUREMENT

Laser-driven photocathode electron sources are essential components of modern advanced x-ray generation systems, including free-electron lasers (FELs), instruments for ultrafast electron diffraction (UED) and dynamic transmission electron microscopy (DTEM). In all these applications, the ultimate performance is determined and limited by the transverse emittance of the electron beam at the photocathode. The emittance is typically defined as a quantity that remains invariant under acceleration to relativistic energies, referred to as the normalized emittance:

$$\text{So, } \varepsilon_{n,rms} = \frac{1}{mc}\sqrt{\langle x^2\rangle\langle p_x^2\rangle} = \frac{\sigma_x\sqrt{\langle p_x^2\rangle}}{mc}, \qquad (1)$$

where σ_x is the rms transverse size of the beam, p_x is the transverse momentum, m is the electron mass and c the speed of light. Eq. (1) suggests that emittance can, in principle, be reduced indefinitely by decreasing the beam size. However, in practice, this reduction is fundamentally limited by space-charge effects. As a result, for practical applications, lowering the transverse momentum is the only effective route to minimizing emittance. For many light source applications, such as FELs, achieving a normalized emittance below 0.5 μm/mm is a critical performance target. Using the three-step framework, Dowell and Schmerge [1] expressed the normalized emittance in terms of the mean transverse energy (MTE) and quantum efficiency (QE) as:

$$MTE(\lambda) = \frac{E_{excess}}{3}, \qquad QE(\lambda) \propto E_{excess}^2, \qquad (2)$$

where $E_{excess} = \hbar\omega - \theta$ with $\hbar\omega$ being the photocathode illumination photon energy and ϕ the photocathode work function. This model was later extended by Vecchione [2] to account for the effects of photocathode temperature and further refined by Saha [3] to include the influence of surface disorder (roughness). The temperature dependence of the rms transverse momentum is illustrated in Fig. 1, reproduced from [2]. The figure shows that reducing the photocathode temperature leads to a lower rms transverse momentum. Exploiting near-threshold photoemission at cryogenic temperatures has enabled record-low energy spreads, such as the 5 meV value reported for a copper photocathode [4].

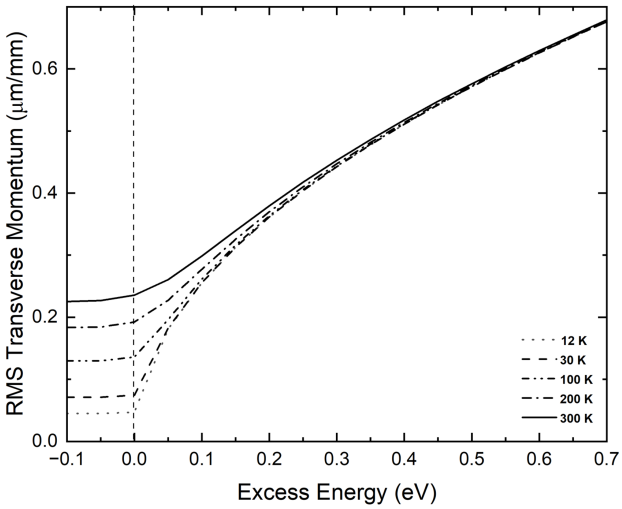

Figure 1: The effect of excess energy and temperature on transverse momentum during photoemission.

The primary motivation for developing these instruments is to identify photocathodes exhibiting low rms transverse

* gowri@slac.stanford.edu
† lee.jones@stfc.ac.uk

ISBN: 978-3-95450-262-2 ISSN: 2673-5350 doi: 10.18429/JACoW-IBIC2025-MOBI01

momentum. Such instruments enable characterization of photocathode emission as a function of illumination wavelength and temperature, examples of which include the cryogenic Momentatron [5] and the Transverse Energy Spread Spectrometer (TESS) [6, 7].

LCLS-II PHOTOCATHODE DEPOSITION CHAMBER

The LCLS-II photocathode deposition system shown in Fig. 2 includes a particle-free load-lock, air-lock, and a photocathode transport suitcase connected to the air-lock, all maintained under extreme high vacuum (XHV) conditions. The growth chamber is equipped with four physical vapor deposition (PVD) sources that support a variety of chemical species and allow for both sequential and co-deposition processes. Photocathodes are deposited onto molybdenum INFN-type plugs, with a 3 mm diameter active area defined by an aperture positioned in front of the cathode. During Cs_2Te growth, the photocathode is illuminated at 258 nm to monitor QE, while quartz crystal microbalances (QCMs) are used to estimate the deposited material thickness. The resulting Cs_2Te photocathodes typically exhibit QE values exceeding 10 %, and remain stable for several months in the transport suitcase under XHV conditions. Notably, the most recent Cs_2Te photocathode, BF01, operated for approximately 1,054 hours, during which its QE gradually degraded from around 8 % to 5 %, but remained sufficient to support beam delivery throughout this period.

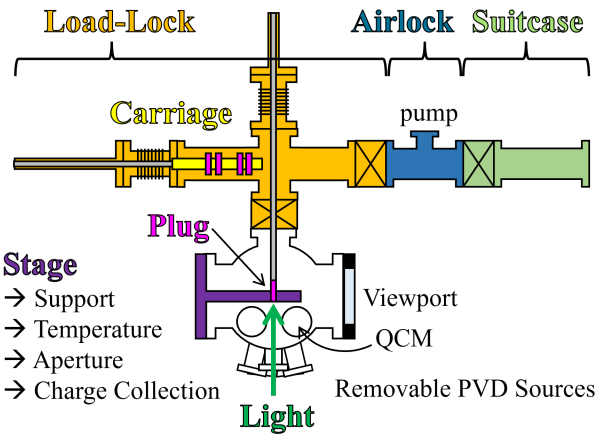

Figure 2: Schematic of the LCLS-II Cs_2Te photocathode deposition system at SLAC.

THE CRYOGENIC MOMENTATRON

The Cryogenic Momentatron at SLAC is specifically designed to characterize photocathode performance for the LCLS-II prior to operational deployment. In addition to qualification measurements, the system provides critical data for developing advanced photoemission models, including the influence of phonons and carriers on the emission process, as well as the effects of residual gas molecule physisorption

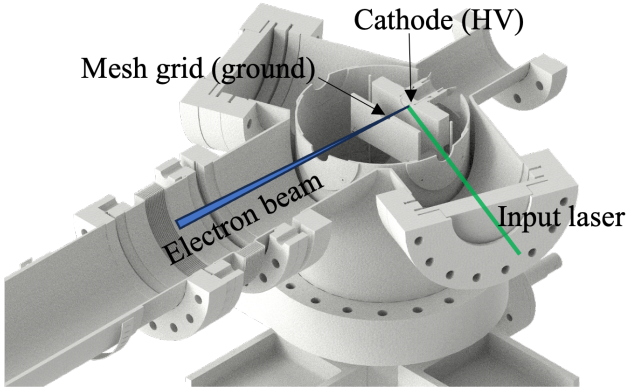

Figure 3: Schematic of the Cryogenic Momentatron.

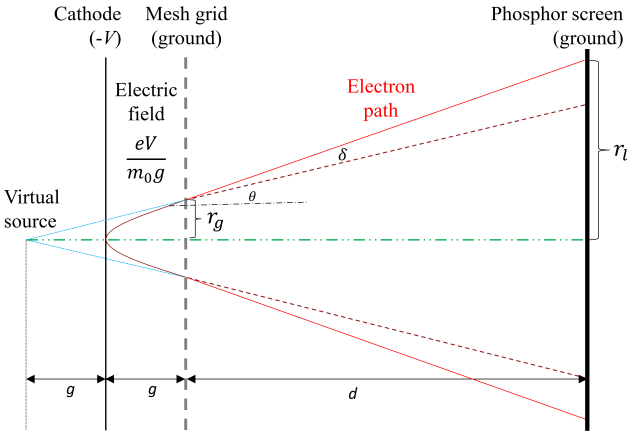

Figure 4: Schematic of the system used to measure transverse momentum. V = applied voltage, 20 kV maximum; g = cathode-anode (grid) gap, 0.020 m; r_g = radial coordinate on the grid w.r.t. nearest grid hole center; δ = angular kick from the mesh-lensing effect; d = drift distance, 0.980 m; r_l = photoelectron radial coordinate on the detector, < 5 mm.

on quantum efficiency (QE) and mean transverse energy (MTE) which is directly related to transverse momentum.

The physical layout of the system is shown in Fig. 3. The Momentatron's load-lock chamber allows connection to a photocathode transport suitcase and uses magnetic transfer arms to move cathodes from the suitcase to the plug holder. The measurement head comprises a stretched electroformed mesh grid mounted in a ring, a sapphire electrical isolator, temperature sensors, and a grounded metal cylindrical body that supports the cathode plug receiver. The photocathode holder is connected to a high-voltage feedthrough, with the mesh grid and cylindrical body held at ground potential.

On the mesh side, electrons accelerated through the grid drift to a microchannel plate–phosphor image intensifier, and the resulting light is recorded by a cooled Andor Xion 888 EMCCD camera (1024 × 1024 pixels, 13 µm pixel size). A dipole magnet near the chamber deflects the drifting electron beam to place it within the camera's field of view. Photocathodes are cooled using an Advanced Research Systems DE-215 cryocooler which provides 30 W of cooling at 45 K and 1.5 W at 4.2 K.

ISBN: 978-3-95450-262-2 ISSN: 2673-5350 doi: 10.18429/JACoW-IBIC2025-MOBI01

The concept of the measurement system is illustrated in Fig. 4. Electrons photoemitted from the cathode are accelerated by a cathode–anode voltage V applied across a small gap g toward a mesh grid anode. The electrons pass through the grid and then drift over several hundred millimeters to a detector. In this setup, the photocathode is typically held at a negative potential, while the grid and detector are grounded.

Within the cathode–anode gap, electrons follow parabolic trajectories and reach the grid with a lateral position r_g and an angle θ. Upon traversing the grid, the electrons experience an additional angular deviation δ due to the mesh grid lensing effect, analogous to the Davisson and Calbick lens phenomenon, as described by Yu *et al.* [8]. This lensing effect can be approximated by

$$\delta = \frac{r_g}{8g},$$

where r_g is the radial coordinate relative to the nearest grid hole center, and g is the cathode–anode gap.

After passing through the grid, the electron beam drifts toward the detector. The radial coordinate of electrons on the detector, r_l, is related to their transverse momentum p_x, the cathode–grid gap g, the drift distance d, and the applied voltage V by the relation Eq. (3)

$$p_x = \frac{r_l}{2g + d}\sqrt{2m_0 eV}. \tag{3}$$

For the chosen parameters, the intrinsic emittance can be estimated from the root-mean-square radial coordinate of electrons on the detector (r_{rms}) as

$$\varepsilon_{\mathrm{int}}\ [\mu\mathrm{m/mm}] \equiv \frac{\varepsilon_{n,\mathrm{rms}}}{\sqrt{\langle x^2 \rangle}} \approx 0.061\sqrt{V\ [\mathrm{kV}]}\ r_{\mathrm{rms}}\ [\mathrm{mm}].$$

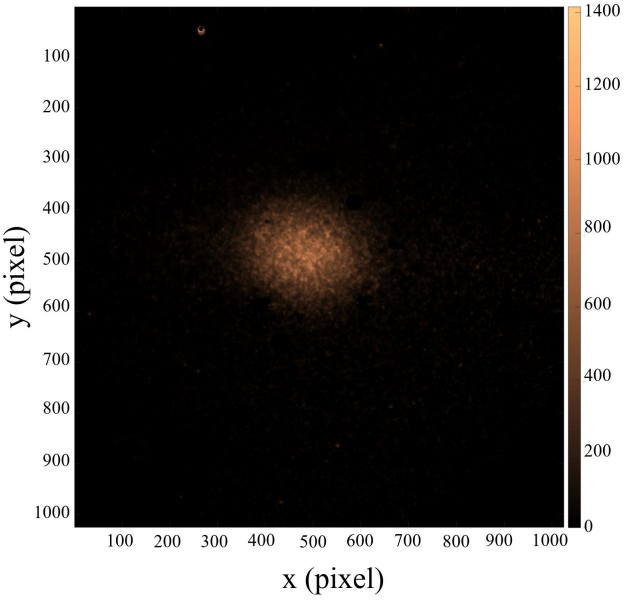

Figure 5: Measured electron beam image at the CCD detector for a copper cathode with a 7 kV accelerating voltage and 4.542 eV photon energy (λ = 273 nm), g = 0.020 m and d = 0.980 m. The Intrinsic emittance is 0.32 µm/mm.

CRYOGENIC MOMENTATRON RESULTS

To test the system, a copper cathode was inserted into the chamber. Illumination was provided by light from a high-power xenon arc lamp coupled to a monochromator, which was fiber-coupled to deliver photons onto the cathode, inducing photoemission.

Figure 5 shows a typical measured round electron beam image on the CCD detector at an accelerating voltage of 7 kV and a photon energy of 4.542 eV (λ = 273 nm). In other measurements, the beam diameter was seen to decrease as the photon energy approached the cathode work function. Additionally, the beam width at the detector can be controlled by varying the acceleration voltage, which is typically adjustable between 1 and 20 kV.

Preliminary data obtained using the Cryogenic Momentatron system are presented in Fig. 6. The experimental results clearly indicate that reducing the temperature results in lower intrinsic emittance, particularly as the excess energy approaches zero in the region close to the photoemission threshold. A substantial amount of additional data has been taken using the Cryogenic Momentatron to study a number of photocathode / photoemissive systems, but this has not yet been fully analyzed. Publication of this work is expected in the coming months.

More comprehensive data will be collected in the future using an NKT Supercontinuum laser which provides illumination wavelengths from 265 nm to over 2000 nm, with pulse lengths under 2 ns and a repetition rate ranging from 1 Hz to 20 kHz.

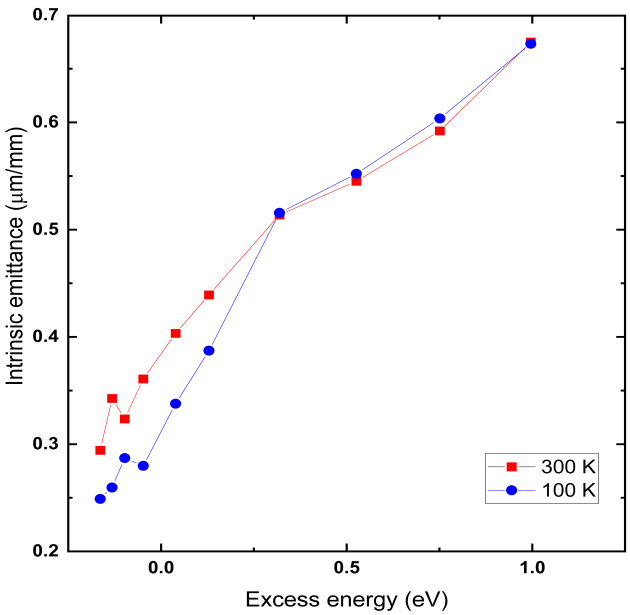

Figure 6: Variation in the intrinsic emittance as a function of excess energy for a copper cathode at temperatures of 100 K and 300 K, with a 7 kV accelerating voltage and a 4.542 eV photon energy (λ = 273 nm), g = 0.020 m and d = 0.980 m.

ISBN: 978-3-95450-262-2 ISSN: 2673-5350 doi: 10.18429/JACoW-IBIC2025-MOBI01

THE TESS SYSTEM

The TESS system [6, 7] shown conceptually in Fig. 7 has been developed separately to, but bears many similarities to the Momentatron systems [5]. Both systems exploit the transverse displacement from an axial reference path of multiple non-relativistic electrons to generate a measureable photoemission footprint from which the transverse energy (momentum) component is extracted. Notable differences are the typical cathode–anode operating potential differences which are 50 – 100 V in TESS compared to 1 – 20 kV for the Momentatron, and the distances through which the electrons propagate. While the Momentatron uses either a xenon arc lamp or a pulsed laser system for cathode illumination, the TESS uses a broadband laser–driven plasma lightsource[1] and monochromator[2] combination to provide a tunable CW light source for photocathode illumination. Like the Cryogenic Momentatron, the TESS system incorporates a liquid nitrogen cooling loop which can reduce the photocathode temperature to around 190 K, so reducing the minimum energy spread (or *thermal floor*) fixed by k_BT from around 25 meV at room temperature to around 18 meV. The TESS also features a piezo–electric fine leak valve which has facilitated detailed studies of photocathode response to controlled degradation to poisoning gas species which modify the surface electronic structure, and hence the photoemission properties. TESS has been used to study photocathode physics for semiconductors, both GaAs [9–11] and Cs_2Te [12, 13], and also for metals [14–17]. The data provided by TESS has improved our understanding of photocathode and photoemission physics, particularly the semiconductor class.

Figure 8 shows the impact on photoemission characteristics for a Cs_2Te photocathode under illumination at a constant wavelength of $\lambda = 266$ nm while subjected to progressive degradation firstly by nitrogen (the control) and then by oxygen (the poison) [13]. The plot demonstrates that the photocathode characteristics do not change under prolonged exposure to nitrogen as this gas species is inert, but that exposure to oxygen (a reactive species) drives an immediate change in both MTE and QE. The data show a progressive evolution in photoemission properties during the integrated exposure to more than 70 L of oxygen, with the MTE increasing while the QE falls. The fundamental emission properties of any Cs_2Te photocathode must therefore change during prolonged operation in a photoinjector electron source. This is highly undesirable, but exposure to residual oxygen is unavoidable in any practical vacuum system.

Figure 9 illustrates the impact of this degradation on the 'clean' and 'degraded' performance of the Cs_2Te photocathode [13]. The data show how the MTE and QE vary as a function of illumination wavelength, λ, and includes Dowell-Schmerge fits [1]. These imply a work function of slightly less than 4.0 eV for the 'clean' photocathode which is higher than the accepted value of 3.5 eV for Cs_2Te, based on a 3.3 eV bandgap with a 0.2 eV positive electron affinity [18], falling to something close to 3.5 eV once degraded by exposure to oxygen. The plot also shows that photoemission is detected under illumination wavelengths far beyond the expected photoemission threshold of 3.5 eV ($\lambda = 350$ nm), albeit with extremely low and eventually vanishing levels of QE. The data demonstrates two challenges encountered when depositing Cs_2Te photocathodes. Firstly, the difficulty in creating just the Cs_2Te compound as Cs and Te are known to form a family of compounds Cs_xTe_y which have different work functions [19–21]. Secondly, the consequence of incorrect stoichiometric ratios during deposition resulting in an excess of Cs in the photoemissive layer which duly reacts with residual oxygen to yield CsO. Both Cs and CsO have very low workfunctions and so generate measurable emission in the TESS at 532 nm. This problem can be mitigated through the use of a multi-wavelength QE monitoring system during photocathode deposition [22]. Such a system provides QE at a number of different sequential wavelengths such as 405 nm and 532 nm, with any measurable photocurrent at these longer wavelengths highlighting deviations from correct stoichiometry arising from an excess of caesium.

FUTURE WORK AND CONCLUSIONS

Future upgrades to the TESS would include improved photocathode cooling to access lower temperatures, with increased light flux at shorter illumination wavelengths, specifically in the range 230 to 260 nm. Accurate measurement of the optical power reflected by the photocathode would add the ability to determine photocathode reflectivity and so assess the impact of surface modifications to increase photon absorption, and thereby QE. The ability to directly measure absolute QE in-situ is also a future aspiration.

The results presented in this paper demonstrate the importance of understanding the subtle behaviors of photocathodes of all classes, and recognizing that their performance is not a constant during accelerator operation. We hope that the importance of the continued development of systems such as the Cryogenic Momentatron and TESS is self–evident to support progress towards the generation of electron beams with the highest possible levels of brightness.

ACKNOWLEDGEMENTS

This material is based upon work supported by the U.S. Department of Energy, Office of Science, Office of Workforce Development for Teachers and Scientists, Office of Science Graduate Student Research (SCGSR) program. The SCGSR program is administered for the DOE by the Oak Ridge Institute for Science and Education under contract No. DE-SC0014664.

This work was also supported by the U.S. Department of Energy under Award No. DE-SC0020387, and by the STFC through their Doctoral Training Studentship programme and the Cockcroft Institute Core Grant No. ST/G008248/1.

[1] Energetiq EQ-99X Laser-Driven Light Source
[2] Bentham TMc300 Single Monochromator

ISBN: 978-3-95450-262-2 ISSN: 2673-5350 doi: 10.18429/JACoW-IBIC2025-MOBI01

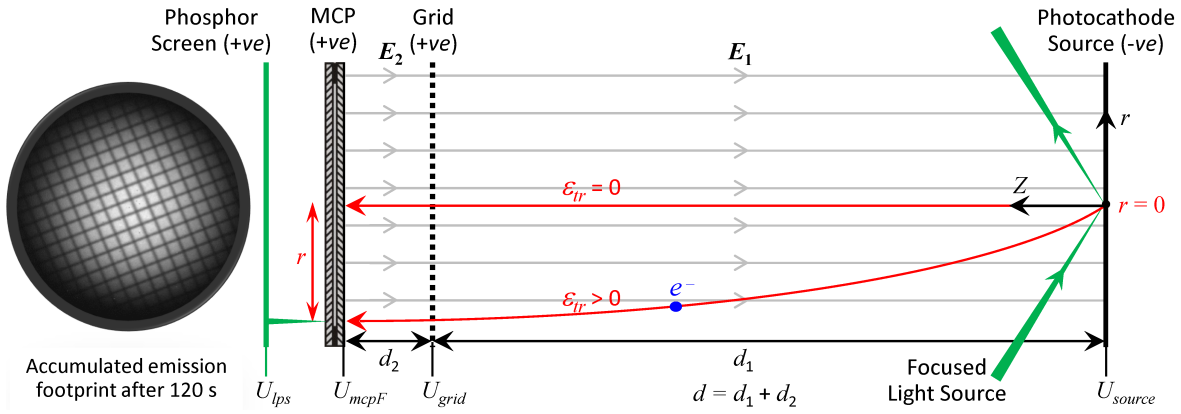

Figure 7: TESS concept to measure the transverse energy component (ε_{tr}) for a single electron from the photoemission footprint generated by $\approx 10^7$ electrons accumulated over a period of 120 s with a typical footprint shown to the left [7].

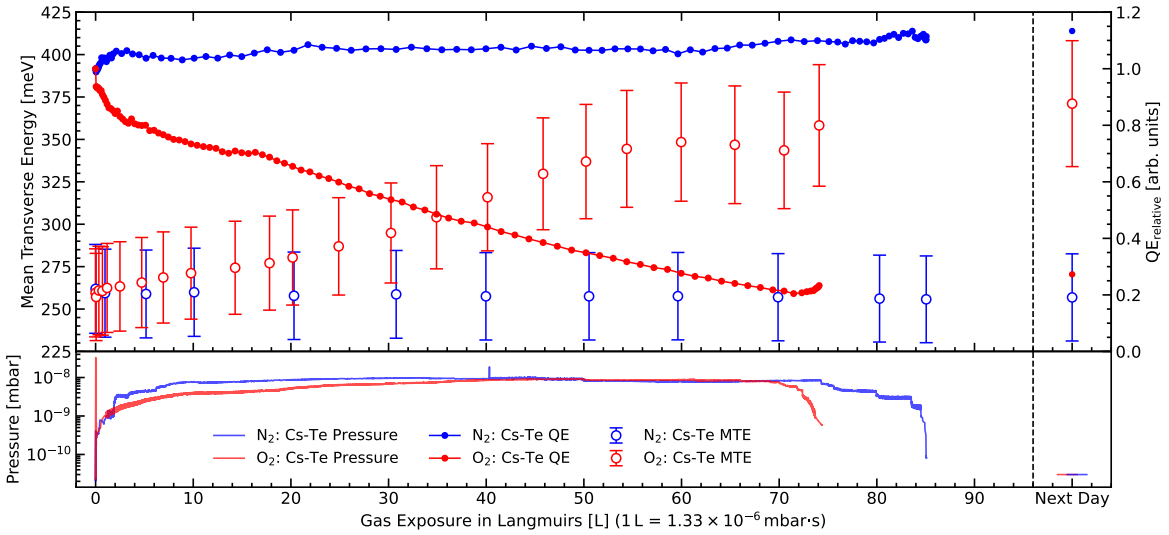

Figure 8: MTE (◦ & ◦, left axis) and relative QE (• & •, right axis) for a Cs_2Te photocathode illuminated at $\lambda = 266$ nm and subjected to progressive degradation by more than 70 L of oxygen (**red data**) and nitrogen (**blue data**) [13].

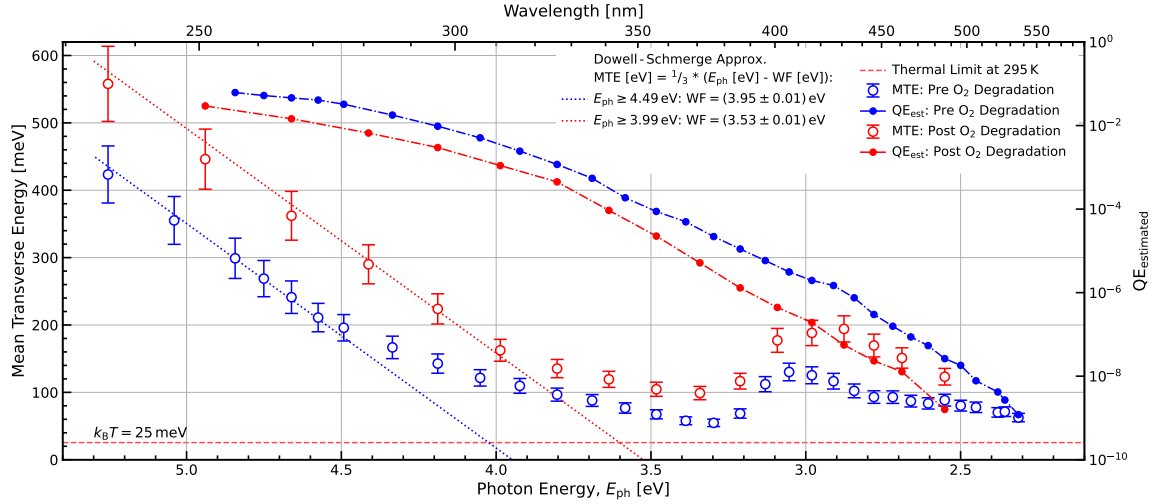

Figure 9: MTE (◦ & ◦, left axis) and estimated QE (• & •, right axis) for a Cs_2Te photocathode under illumination with $\lambda = 236$ to 536 nm before degradation (**blue data**) and after degradation (**red data**) by more than 70 L of oxygen [13].

ISBN: 978-3-95450-262-2 ISSN: 2673-5350 doi: 10.18429/JACoW-IBIC2025-MOBI01

REFERENCES

[1] D. H. Dowell and J. F. Schmerge, "Quantum efficiency and thermal emittance of metal photocathodes", *Phys. Rev. Spec. Top. Accel. Beams*, vol. 12, p. 074201, 2009. doi:10.1103/PhysRevSTAB.12.074201

[2] T. Vecchione *et al.*, "Quantum Efficiency and Transverse Momentum From Metals", in *Proc. FEL'13*, New York, NY, USA, Aug. 2013, paper TUPSO83, pp. 424–426.

[3] P. Saha *et al,*, "Theory of photoemission from cathodes with disordered surfaces", *J. Appl. Phys.*, vol. 133, p. 053102, 2023. doi:10.1063/5.0135629

[4] S. Karkare *et al.*, "Ultracold Electrons via Near-Threshold Photoemission from Single-Crystal Cu(100)", *Phys. Rev. Lett.*, vol. 125, p. 054801, 2020. https://doi.org/10.1103/PhysRevLett.125.054801

[5] J. Feng *et al.*, "A novel system for measurement of the transverse electron momentum distribution from photocathodes", *Rev. Sci. Instrum.*, vol. 86, p. 015103, 2015. doi:10.1063/1.4904930

[6] L. B. Jones *et al.*, "The Commissioning of Tess: An Experimental Facility for Measuring the Electron Energy Distribution From Photocathodes", in *Proc. FEL'13*, New York, NY, USA, Aug. 2013, paper TUPSO33, pp. 290–293.

[7] L. B. Jones, *et al.*, "The measurement of photocathode transverse energy distribution curves (TEDCs) using the transverse energy spread spectrometer (TESS) experimental system", *Rev. Sci. Inst.*, vol. 93, p. 113314, 2022. doi:10.1063/5.0109053

[8] L. Yu, W. Wan, W.X. Tang, and J. Feng, "Systematic analysis of a compact setup to measure the photoemitted electron beam transverse momentum and emittance", *Rev. Sci. Instrum.*, vol. 92, p. 013302, 2021. doi:10.1063/5.0013122

[9] L. B. Jones *et al.*, "Evolution of the transverse and longitudinal energy distributions of electrons emitted from a GaAsP photocathode as a function of its degradation state", *J. Appl. Phys.*, vol. 121, p. 225703, 2017. doi:10.1063/1.4984603

[10] L. B. Jones *et al.*, "Non–monotonic behaviour in the mean transverse energy of electrons emitted from a reflection–mode p-GaAs(Cs,O) photocathode during its QE degradation through oxygen exposure", *J. Phys. D: Appl. Phys.*, vol. 54, p. 205301, 2021. doi:10.1088/1361-6463/abe1e9

[11] W. Andreas Schroeder, L. A. Angeloni, I.-J. Shan, and L. B. Jones, "Franck-Condon electron emission from polar semiconductor photocathodes", *Phys. Rev. Appl.*, vol. 23, p. 054065, 2025. doi:10.1103/PhysRevApplied.23.054065

[12] L. B. Jones *et al.*, "Mean transverse energy, surface chemical and physical characterization of CERN-made Cs-Te photocathodes", *Phys. Rev. Accel. Beams*, vol. 27, p. 023402, 2024. doi:10.1103/PhysRevAccelBeams.27.023402

[13] H. Churn, L. Jones, and T. Noakes, "Mean Transverse Energy and Degradation Measurements on a Caesium Telluride Photocathode", in *Proc. IPAC'23*, Venice, Italy, May 2023, pp. 1404–1407. doi:10.18429/JACoW-IPAC2023-TUPA030

[14] D. P. Juarez-Lopez, "Characterisation of High–Performance Electron Sources for Particle Accelerators using a Transverse Energy Spread Spectrometer", Ph.D. thesis, University of Liverpool, UK, 2021.

[15] L. A. J. Soomary, L. B. Jones, D. P. Juarez-Lopez, T. C. Q. Noakes, and C. P. Welsch, "Performance Characterisation of a Cu (100) Single-Crystal Photocathode", in *Proc. IPAC'21*, Campinas, Brazil, May 2021, pp. 2860–2862. doi:10.18429/JACoW-IPAC2021-WEPAB112

[16] C. Benjamin *et al.*, "Enhanced performance of an Ag(100) photocathode by an ultra-thin MgO film", *J. Appl. Phys.*, vol. 132, p. 195303 doi:10.1063/5.0124528

[17] L. Jones, C. Welsch, L. Soomary, R. Valizadeh, and T. Noakes, "Characterisation of a Cs-implanted Cu photocathode", in *Proc. IPAC'23*, Venice, Italy, May 2023, pp. 1611–1614. doi:10.18429/JACoW-IPAC2023-TUPA138

[18] S. H. Kong, J. Kinross-Wright, D. C. Nguyen, and R. L. Sheffield, "Cesium telluride photocathodes", *J. Appl. Phys.*, vol. 77, pp. 6031–6038, 1995. doi:10.1063/1.359188

[19] J. McFarlane, and J. C. LeBlanc, "Fission-Product Tellurium and Cesium Telluride Chemistry Revisited", Atomic Energy of Canada Ltd., Whiteshell Laboratories, Pinawa, Manitoba, Canada, Rep. AECL-11333, COG-95-276-I, 1996. https://inis.iaea.org/collection/NCLCollectionStore/_Public/29/054/29054591.pdf

[20] A. Band *et al.*, "Characterization of Oxides of Cesium", *J. Phys. Chem. B*, vol. 108, pp. 12360–12367, 2004. doi:10.1021/jp036432o

[21] A. Ruth *et al.*, "Searching for low-workfunction phases in the Cs-Te system: The case of Cs_2Te_5", *J. Appl. Phys.*, vol. 113, p. 183703, 2013. doi:10.1063/1.4804155

[22] L. Monaco, P. M. Michelato, C. Pagani, and D. Sertore, "On-Line Diagnostic during Cs2Te Photocathodes Formation", in *Proc. PAC'09*, Vancouver, Canada, May 2009, paper MO6RFP072, pp. 536–538.